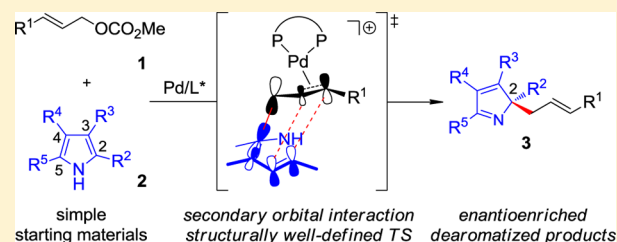# Mechanistic Insights into the Pd-Catalyzed Intermolecular Asymmetric Allylic Dearomatization of Multisubstituted Pyrroles: Understanding the Remarkable Regio- and Enantioselectivity

Chao Zheng,* Chun-Xiang Zhuo, and Shu-Li You*

State Key Laboratory of Organometallic Chemistry, Shanghai Institute of Organic Chemistry, Chinese Academy of Sciences, 345 Lingling Lu, Shanghai 200032, China

Ⓢ *Supporting Information*

ABSTRACT: In this article we report a comprehensive density functional theory study on the Pd-catalyzed intermolecular asymmetric allylic dearomatization reactions of multisubstituted pyrroles. The calculated results are in line with the previous experimental observations (*J. Am. Chem. Soc.* **2014**, *136*, 6590), and the remarkable regio- and enantioselectivity are well explained. Of all the potential nucleophilic sites around the multisubstituted pyrrole ring, the reaction always occurs at the position where the HOMO of the molecule distributes most significantly. In contrast

to the common view on the enantioselectivity of the Pd-catalyzed asymmetric allylic substitution reactions, we find that the steric interaction between the nucleophile and the chiral ligand does not have the dominating effect on the enantioselectivity of the reaction. Instead, the interaction between the allyl moiety and the incoming nucleophile plays an important role in the enantioselectivity-determining process.

■ INTRODUCTION

To achieve high levels of chemo-, regio-, and stereoselectivity in developing novel synthetic methodology is a central topic of modern organic chemistry and at the same time a basic requirement for reaching the goal of ideal synthesis.[1] Undoubtedly, in the field of asymmetric catalysis, a deep understanding of the origin of stereoselectivity is of great importance in devising highly enabling synthetic methods. However, the stereoselectivity usually stems from subtle non-covalent interactions between the chiral catalyst and the substrates in the activated complex that cannot be directly observed by traditional experimental methods. In this regard, density functional theory (DFT) calculations play an increasingly important role in probing the mechanistic details in asymmetric catalysis.[2]
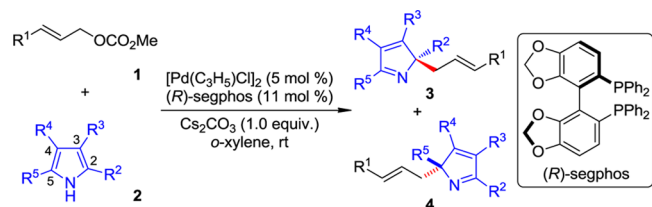
Thanks to intensive investigations for several decades, Pd-catalyzed asymmetric allylic substitution[3] has evolved into a robust and reliable method for the construction of C—C and C—X bonds in a highly stereoselective manner. Among various nucleophiles compatible with this type of transformation, the reactions involving prochiral carbon nucleophiles such as β-dicarbonyl compounds and analogues,[4] ketone enolates and analogues,[5] enol silyl ethers,[6] and azalactones[7] are attractive since a chiral center will be established in the incoming nucleophile moiety.[8,9] Typically, application of the Trost ligands results in excellent enantioselectivity for these reactions.[10] It is generally accepted that it is possible to reach high enantioselectivity for these systems due to the very deep chiral pocket generated by the ligand, which allows the phenyl groups of the ligand to influence the approaching trajectory of

the incoming nucleophile on the opposite side. Besides, the amide moieties of the ligand have also been suggested to interact with the nucleophile via hydrogen-bonding or electrostatic interactions.[11] However, further mechanistic investigations supported by DFT calculations in pursuit of a deeper understanding of the issue of enantioselectivity in Pd-catalyzed asymmetric allylic substitution reactions still remain in great demand.[12]

In recent years, aromatic rings have been proved applicable as versatile nucleophiles in transition-metal-catalyzed asymmetric allylic substitution reactions. However, in most cases, the chiral centers can only be installed in the allyl moiety because the substitution of the aryl C—H bonds with an allyl group cannot interrupt the sp² hybridization at the nucleophilic site of arenes. Alternatively, it has been found that substituted arenes can be used as prochiral nucleophiles, leading to asymmetric allylic dearomatization reactions.[13] In this context, an intra-molecular design is usually necessary to obtain enhanced stereochemical control via a conformationally restricted transition state. Although diverse fused or spiro polycyclic scaffolds can be accessed in this way, the current methodologies still suffer from tedious syntheses of the substrates and limited scope. In order to address these drawbacks, highly efficient intermolecular asymmetric allylic dearomatization reactions are highly desired, but successful examples are rare in the literature.[14]

Table 1. Pd-Catalyzed Intermolecular Asymmetric Allylic Dearomatization Reaction of Multisubstituted Pyrroles[a]

entry	1, R^1	2, R^2, R^3, R^4, R^5	$3/4^b$	combined yield of 3 and 4 (%)	ee of 3 (%)^c
1	**1a**, Ph	**2a**, Me, H, H, Me	/	85	89
2	**1a**, Ph	**2b**, Me, Me, H, Me	95/5	85	95
3	**1a**, Ph	**2c**, Me, ^{n}Bu, H, Me	95/5^d	85	95
4	**1a**, Ph	**2d**, Me, ^{c}Pr, H, Me	>95/5	90	91
5	**1a**, Ph	**2e**, Me, Ph, H, Me	94/6	86	91
6	**1a**, Ph	**2f**, Me, *p*-Tol, H, Me	93/7	93	94
7	**1a**, Ph	**2g**, Me, *p*-OMeC$_6$H$_4$, H, Me	92/8	86	91
8	**1a**, Ph	**2h**, Me, *p*-FC$_6$H$_4$, H, Me	95/5	95	93
9	**1a**, Ph	**2i**, Me, Me, H, Ph	>95/5	90	95
10	**1a**, Ph	**2j**, Me, Me, Me, Me	/	78	91
11	**1a**, Ph	**2k**, Me, Me, Ph, Me	76/24	92	93
12	**1b**, *p*-Tol	**2b**, Me, Me, H, Me	94/6	84	92
13	**1c**, 2-thienyl	**2b**, Me, Me, H, Me	94/6	77	97 (R)

[a]Reaction conditions: 0.4 mmol of **1**, 0.2 mmol of **2**, 0.2 mmol of Cs$_2$CO$_3$, 5 mol % of [Pd(C$_3$H$_5$)Cl]$_2$, and 11 mol % of (*R*)-segphos in 2.0 mL of *o*-xylene at rt. [b]The ratio of **3/4** was determined by ^{1}H NMR analysis of the crude reaction mixture. [c]ee of **3** was determined by HPLC analysis. [d]Determined by GC analysis of the crude reaction mixture.

Recently, we developed a Pd-catalyzed intermolecular asymmetric allylic dearomatization reaction of multisubstituted pyrroles (Table 1).[15,16] In the presence of a catalytic amount of Pd-complex ligated by (*R*)-segphos, an array of multisubstituted pyrroles **2** was found to be reactive toward monosubstituted allylic carbonates **1** to yield dearomatized multisubstituted 2*H*-pyrroles **3**. This reaction exhibits remarkable multiple selectivities. For 2,5-dimethylpyrrole **2a**, the reaction occurs exclusively at the C2 position, leaving the unsubstituted C3 position intact (entry 1). For a series of 2,3,5-trisubstituted pyrroles **2b−i**, the reactions take place at the sterically more hindered C2 position (entries 2−9, 12, and 13). For all the substrates tested, *N*-allylation has never been observed. Note that a high level of enantioselectivity was obtained with an axially chiral bisphosphine ligand which has not been utilized in the Pd-catalyzed asymmetric allylic substitution reactions with substituted arenes as the prochiral nucleophiles.[17]

Herein, we report our detailed mechanistic observations of this novel reaction, with an emphasis on revealing the origins of the aforementioned multiple selectivities. The results of the DFT calculations suggest that the distribution of the highest occupied molecular orbital (HOMO) of multisubstituted pyrroles dominates in determining the chemo- (C2 vs N) and regioselectivity (C2 vs C5, C2 vs C4, and C2 vs C3) among the several potential nucleophilic sites. Interestingly, we found the steric interaction between the nucleophile and the chiral ligand does not play a crucial role in determining the enantioselectivity, in contrast to the common view on the enantioselectivity issue of Pd-catalyzed asymmetric allylic substitution reactions. In fact, it is the interaction between the incoming nucleophile and the Pd-allyl complex, especially the secondary orbital interaction between the pyrrole ring and the allyl moiety, which contributes significantly in the chiral discrimination process by forging a well-organized approaching trajectory.

COMPUTATIONAL METHODS

All calculations in this paper were performed with the Gaussian09 package.[18] The DFT method was employed using the M06-2X functional.[19] The SDD basis set with the associated effective core potential was used for Pd and the 6-31+G(d,p) basis set for other atoms. The keyword "5d" was specified to use five pure *d* functions in the calculations. Optimizations were conducted without any constraint using the SMD model[20] in *o*-xylene (ε = 2.5454). Frequency analyses were carried out to confirm that each structure is a local minimum (no imaginary frequency) or a transition state (only one imaginary frequency). The energies were further estimated by single-point calculations using the B3LYP functional,[21] including the D3 version of Grimme's empirical dispersion correction with Becke−Johnson damping.[22] This method often yields reasonable results for non-covalent interactions[23] which are important in asymmetric catalysis. In the single-point calculations, the SDD basis sets with the associated effective core potential was used for Pd and the 6-311++G(d,p) basis sets for other atoms. The Gibbs free energies in *o*-xylene (ΔG), including the single-point corrections, are discussed throughout this paper unless otherwise specified. Fragment distortion and interaction energies were computed at the B3LYP-D3(BJ)/SDD/6-311++G(d,p) level of theory using the M06-2X/SDD/6-31+G(d,p) geometry. Orbital composition analyses were conducted by the natural atomic orbital method with Multiwfn.[24] The 3D images of the calculated structures were prepared using CYLview.[25] The full computational details can be found in the Supporting Information.

RESULTS AND DISCUSSION

General Consideration. The general catalytic cycle of the Pd-catalyzed asymmetric allylic substitution reactions is well known (Figure 1). The catalytically active Pd(0) species first coordinates with the allylic substrate. The subsequent oxidative addition gives rise to the key Pd-allyl intermediate, which is attacked by the nucleophile at the less substituted terminal position. The final ligand exchange releases the desired product and closes the catalytic cycle. Since all kinds of selectivities are determined during the nucleophilic attacking step, the majority of the following calculations will then be focused on this step.
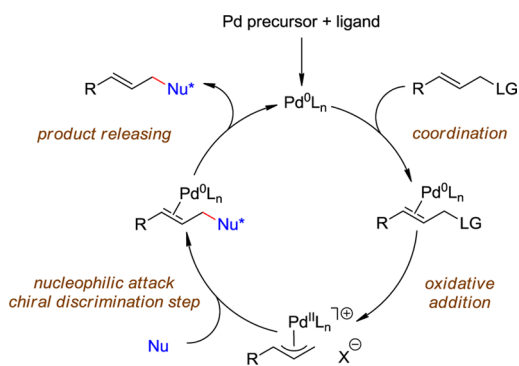
Figure 1. General catalytic cycle.

Configuration of the Pd-Allyl Complex. The reaction between 2-thienyl allyl carbonate **1c** and 2,3,5-trimethylpyrrole **2b** was chosen as the model reaction because the corresponding product **3cb** was delivered in excellent regio-selectivity (**3cb/4cb** = 94/6) and the highest enantioselectivity (97% ee). The structure and the absolute configuration of **3cb** were confirmed unambiguously by X-ray crystallographic analysis. The chiral environment generated by (*R*)-segphos can be described according to the classic quadrant analysis[26] (Figure 2). On coordinating to a Pd center, the chiral ligand shows a highly skewed conformation. Two phenyl groups

which are oriented equatorially extrude toward the Pd center, making the II and IV quadrants sterically more encumbered than the other two quadrants, where the two axially oriented phenyl groups are accommodated at the sides of the biphenyl backbone, thus pointing away from the Pd center. When the 2-thienyl allyl moiety coordinates to the Pd center, two different configurations of the complex (**Pd-allyl-*endo*** or **Pd-allyl-*exo***) can be adopted, and their energies should be different owing to the surrounding chiral environment (in this article, we refer to the configuration in which the C2−H bond of the allyl moiety points toward the +*Y* direction as *endo*, and the other configuration as *exo*). The calculated relative energy of **Pd-allyl-*endo*** is lower than that of **Pd-allyl-*exo*** by 1.1 kcal/mol because the 2-thienyl group in **Pd-allyl-*endo*** is located at the less congested quadrant. More importantly, these two configurations can be further distinguished in the nucleophilic addition step. According to the studies by van Leeuwen and co-workers,[27] the hybridization scenario of C1 switches from sp^2 to sp^3 as the new C−C bond is forming, and the coordination mode of the allyl moiety to the Pd center will change from η^3 to η^2 accordingly. In order to achieve this end, the allyl moiety of **Pd-allyl-*endo*** should rotate in a counterclockwise fashion, posing both the 2-thienyl group and the incoming nucleophile in the less congested quadrants. The situation with **Pd-allyl-*exo*** is just the opposite: a clockwise rotation of the allyl moiety
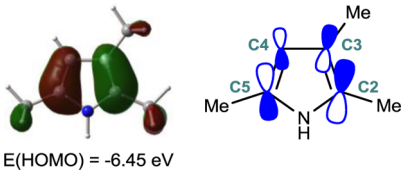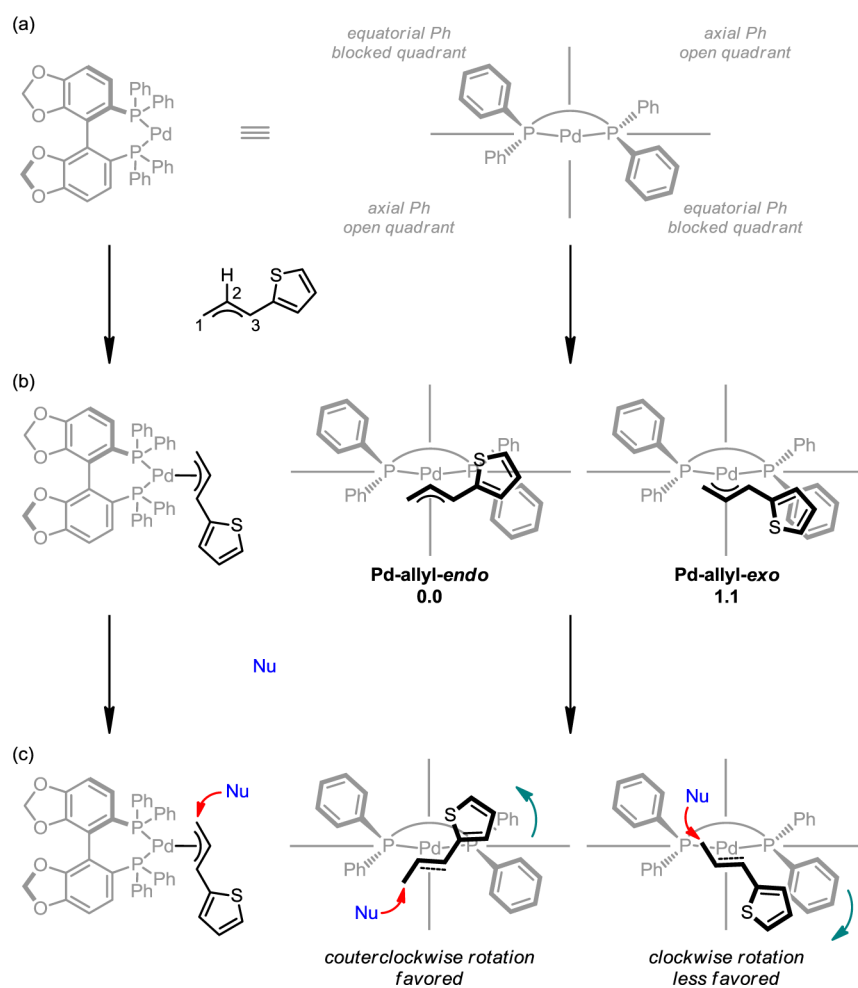

Figure 2. (a) Quadrant analysis of the chiral environment generated by (*R*)-segphos. (b) Simplified structures of **Pd-allyl-*endo*** and **Pd-allyl-*exo***, and their relative energies in kcal/mol. (c) Schematic description of the allyl rotation as the nucleophile is attacking.

forces both the 2-thienyl group and the incoming nucleophile to be in the more congested quadrants. Taking into account the fact that both **Pd-allyl-endo** and **Pd-allyl-exo** are accessible due to the fast $\pi-\sigma-\pi$ transformation of the Pd-allyl complexes,[28] it can be anticipated that the pyrrole nucleophile will attack **Pd-allyl-endo** preferentially.

On the Chemo- and Regioselectivity among the Potential Nucleophilic Sites of Pyrroles. In order to probe the origins of the chemo- and regioselectivity among the potential nucleophilic sites of multisubstituted pyrroles, we conducted orbital composition analysis of the HOMO of 2,3,5-trimethylpyrrole (**2b**) and calculated the relative energetic barriers of the transition states that **2b** attacks the Pd-allyl complex derived from **1c** with different nucleophilic sites. (In these transition states, the Pd-allyl complex is in *endo* configuration; the nucleophile is approaching the Pd-allyl complex in such a trajectory that the pyrrole ring and the allyl moiety overlap with each other in the maximal way, *vide infra*.) The HOMO of **2b** is mainly composed of the $2p_z$ orbitals of the carbon and nitrogen atoms around the aromatic ring. A clear correlation between the HOMO distribution at each nucleophilic site and the relative energetic barrier of the corresponding transition state can be observed, as listed in Table 2. The C2 position is the most nucleophilic site in that

Table 2. Relationship between the HOMO Distribution of 2b and the Chemo- and Regioselectivity

E(HOMO) = -6.45 eV

entry	pyrrole position	HOMO distribution (%)	relative energetic barrier (kcal/mol)
1	N	0.3	13.5
2	C2	33.2	0.0
3	C3	16.8	4.0
4	C4	9.2	4.5
5	C5	29.0	3.5

the contribution of the $2p_z$ orbital of C2 to the HOMO of **2b** is estimated to be 33.2%, the most significant among all the atoms. Accordingly, the attack of the C2 position of **2b** to the Pd-allyl complex enjoys the lowest energetic barrier (entry 2). As the HOMO distribution on a given position decreases (C2 > C5 > C3 > C4 > N), the calculated energy of the transition state for the nucleophilic attack at this position of **2b** to the Pd-allyl complex goes up gradually, with attack at the C5 position being the second most favorable (entry 5). This is well in agreement with the experimentally observed chemo- and regioselectivity (Table 1, entry 13).

To evaluate the generality of the influence of the HOMO distribution of multisubstituted pyrroles to the chemo- and regioselectivity in the Pd-catalyzed intermolecular asymmetric allylic dearomatization reactions, orbital composition analyses were conducted for all the multisubstituted pyrroles (**2a–k**) that have been tested experimentally. The results are summarized in Figure 3. For symmetric substrates 2,5-dimethylpyrrole **2a** and 2,3,4,5-tetramethylpyrrole **2j**, the HOMO distribution at the C2 (or C5) position is much more significant than that at the C3 (or C4) position no matter

whether the C3 and C4 positions are substituted (31.1% vs 14.1% for **2a**; 31.2% vs 12.3% for **2j**), which implies much stronger nucleophilicity at the C2 and C5 positions compared with the C3 and C4 positions for these substrates. On the other hand, the introduction of an alkyl or an aryl substituent at the C3 position to 2,5-disubstituted pyrroles leads to some perturbation of the HOMO distribution at the C2 and C5 positions. The contribution of the $2p_z$ orbital of C2 becomes more significant than that of C5, with the corresponding difference ("Δ value", Figure 3) ranging from 3.1% to 7.7%. These results clearly indicate that the C2 position is the most nucleophilic site of the 2,3,5-trisubstituted pyrroles, and the experimentally observed chemo- and regioselectivity might be mainly determined by the HOMO distribution of the nucleophiles. Notably, for 2,3,5-trimethyl-4-phenylpyrrole **2k**, the difference between the HOMO distribution at the C2 and C5 positions is negligible ($\Delta = -0.2\%$), and the poor regioselectivity (**3k/4k** = 76/24, Table 1, entry 11) might stem from the different steric effects that are caused by 3-methyl and 4-phenyl groups.

On the Enantioselectivity. To realize a high level of enantioselectivity in intermolecular asymmetric allylic dearomatization reactions is not trivial, because the nucleophilic arenes can approach the Pd-allyl complex in a conformationally non-restricted fashion. The existence of a collection of different transition states that are all energetically accessible is usually detrimental for the chiral discrimination process. Experimentally, the BINAP-type bisphosphine ligands have been used in the Pd-catalyzed intermolecular asymmetric allylation of prochiral nucleophiles such as α-acetamido-β-ketoesters, α-amino phosphonates, and α-substituted β-diketones.[17] It was suggested that the phenyl groups of BINAP may interact with the prochiral nucleophile which approaches the π-allyl moiety from the opposite side and the enantioselectivity originates.[17a] However, the detailed mechanism for the enantioface-selection still remains elusive.

To obtain deep insights into the origins of the enantioselectivity of the target reaction, 12 nucleophilic attacking transition states with different approaching trajectories of 2,3,5-trimethylpyrroles to the Pd-allyl moiety were calculated, each of which is a local minimum in the Newman projection. The simplified structures as well as the relative energies of the six transition states in which the Pd-allyl moiety adopts the favorable *endo* configuration are shown in Figure 4. (The other six transition states in which the Pd-allyl moiety adopts the *exo* configuration have much higher energies and thus are less important for the chiral discrimination. See the Supporting Information for details.) The absolute configuration of the dearomatized product is determined by the facial selectivity of the approaching pyrrole ring in the nucleophilic attack step: *Re*-face attack of 2,3,5-trimethylpyrrole will result in (*R*)-product, whereas *Si*-face attack will result in (*S*)-product. Taking all 12 transition states that are considered into account, the formation of (*R*)-product should be favored, and the calculated ee value is 92% by applying the Boltzmann distribution, which is in accord with the experimental observation (97% ee for **3cb**, Table 1, entry 13).

Interestingly, in each series (*Re*-face attack or *Si*-face attack), there is one special transition state whose relative energy is much lower than the other two counterparts. For instance, **TS-endo-Re-(-sc)** (0.0 kcal/mol) is the most stabilized transition state leading to (*R*)-product, while the relative energies of the other two transition states leading to (*R*)-product, **TS-endo-Re-**
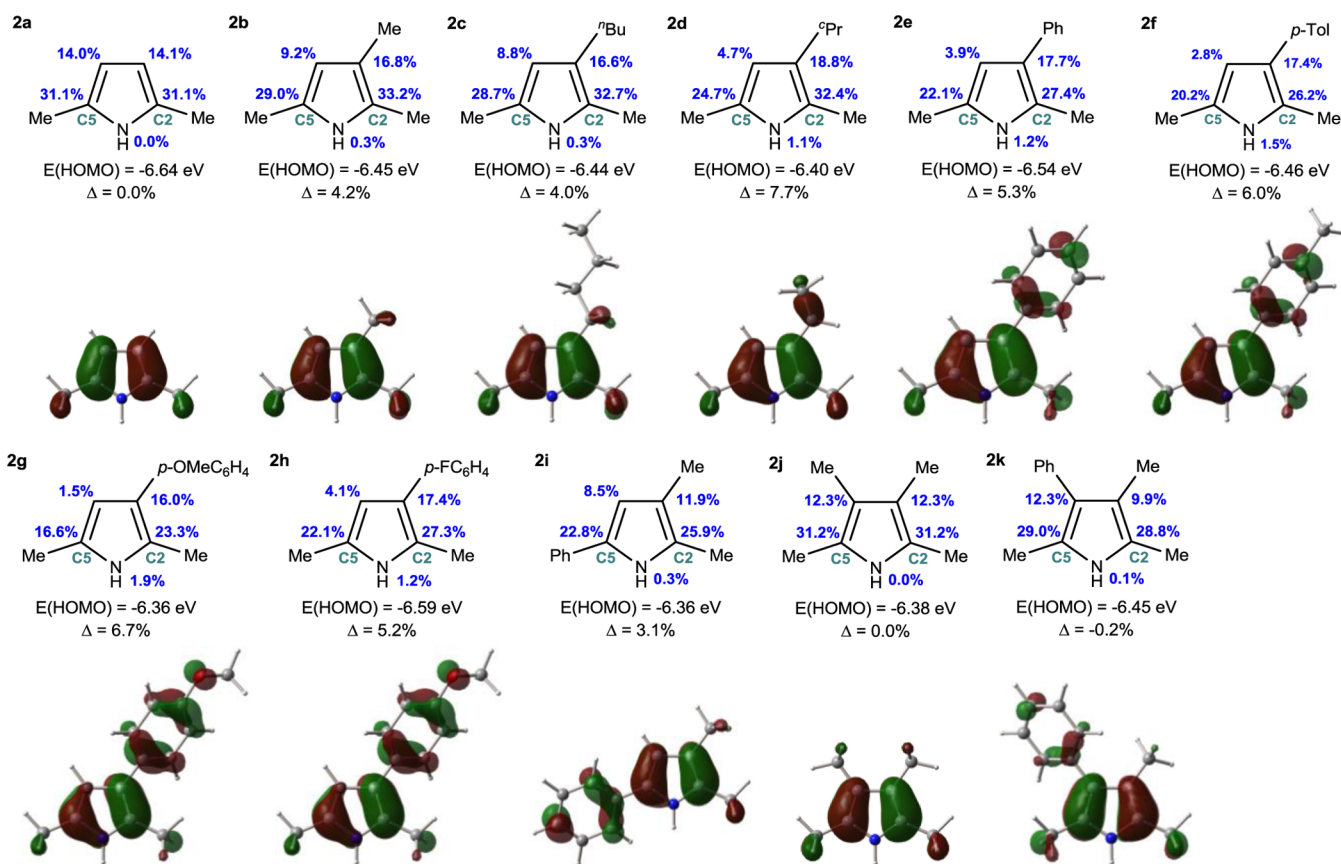
Figure 3. HOMO distribution of multisubstituted pyrroles. The Δ value is defined as the difference between the contributions of $2p_z$ orbitals of C2 and C5 atoms to the HOMO of multisubstituted pyrrole.
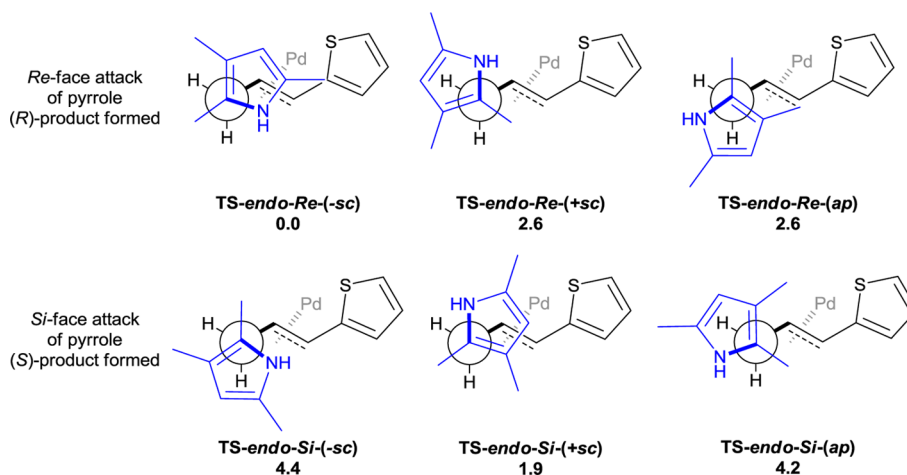
Figure 4. Simplified structures and the relative energies of the six nucleophilic attacking transition states where the Pd-allyl moiety adopts the *endo* configuration. The transition states are named according to the configuration of the Pd-allyl moiety (*endo* or *exo*), the facial selectivity of the pyrrole nucleophile (*Re* or *Si*), and the relative position of the C−C bond of the Pd-allyl moiety and the C−N bond of 2,3,5-trimethylpyrrole which are shown in bold: −*sc* (− *synclinal*), +*sc* (+ *synclinal*) or *ap* (*antiperiplanar*). The energies are in kcal/mol.

(+*sc*) and **TS-endo-Re-(ap)**, are both 2.6 kcal/mol higher. A similar trend can be observed for the three transition states leading to (*S*)-product. The most favorable transition state for *Si*-face attack is **TS-endo-Si-(+sc)** (1.9 kcal/mol), whose energy is also lower than that of the other two transition states, **TS-endo-Si-(-sc)** (4.4 kcal/mol) and **TS-endo-Si-(ap)** (4.2 kcal/mol), by about 2 kcal/mol. These results indicate that although theoretically, a collection of different transition states can be expected for this Pd-catalyzed intermolecular asymmetric allylic

dearomatization of multisubstituted pyrroles, yet only one of them is the most accessible for the formation of (*R*)- and (*S*)-product, respectively, and these two transition states [**TS-endo-Re-(-sc)** and **TS-endo-Si-(+sc)**] contribute the most to the chiral discrimination process.[29]

What makes the two lowest-energy transition states **TS-endo-Re-(-sc)** and **TS-endo-Si-(+sc)** unique compared with other counterparts? We next applied the activation strain model (ASM)[30] to address this issue. ASM is a fragment approach to
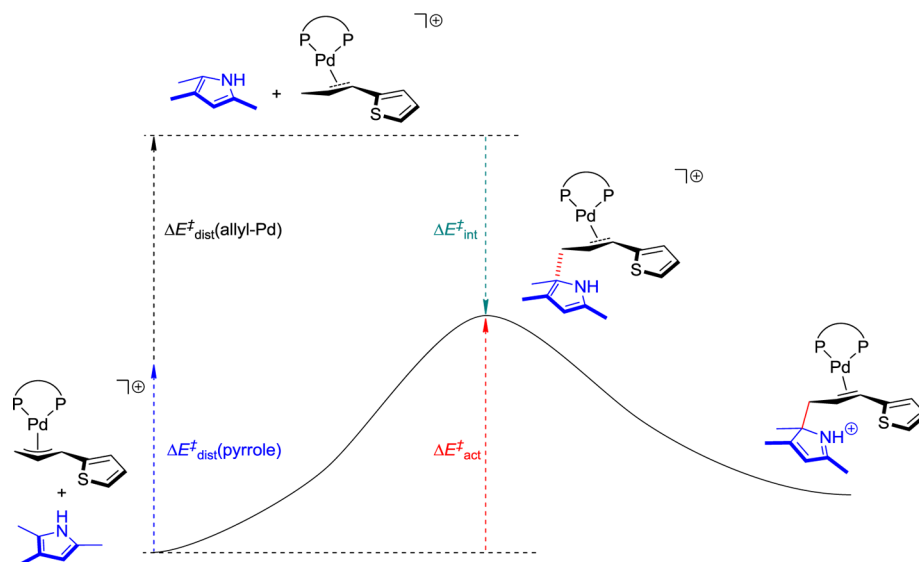
16255

dx.doi.org/10.1021/ja5080135 | *J. Am. Chem. Soc.* 2014, 136, 16251−16259

Figure 5. Relationship between the activation energy and the distortion and interaction energies of reactants.

Table 3. Activation Strain Model Analysis for Nucleophilic Attack Transition States (All Values Are in kcal/mol)

entry	TS	configuration of the product	$\Delta E^{\ddagger}_{dist}$(pyrrole)	$\Delta E^{\ddagger}_{dist}$(Pd-allyl)	$\Delta E^{\ddagger}_{int}$	$\Delta E^{\ddagger}_{act}{}^a$
1	**TS-*endo*-*Re*-(-*sc*)**	(R)	6.3	19.6	−19.4	6.6
2	**TS-*endo*-*Re*-(+*sc*)**	(R)	6.4	18.9	−15.1	10.2
3	**TS-*endo*-*Re*-(*ap*)**	(R)	6.4	20.3	−16.3	10.4
4	**TS-*endo*-*Si*-(-*sc*)**	(S)	6.1	18.8	−15.4	9.5
5	**TS-*endo*-*Si*-(+*sc*)**	(S)	7.0	20.7	−19.8	7.9
6	**TS-*endo*-*Si*-(*ap*)**	(S)	6.4	20.1	−15.8	10.7

^{a}The $\Delta E^{\ddagger}_{act}$ value is the calculated electronic energy of each transition state relative to the sum of the electronic energies of the two separate reactants. The positive $-T\Delta S$ term for a process that generates one product from two reactants is not included. Near room temperature, $-T\Delta S \approx 10$ kcal/mol. The calculated $\Delta G^{\ddagger}$ value of **TS-*endo*-*Re*-(-*sc*)** is 19.6 kcal/mol.[32]

understand organic reactions, in which the height of the energetic barrier is described in terms of the original reactants. As depicted in Figure 5, the activation energy of the transition states of the nucleophilic attack ($\Delta E^{\ddagger}_{act}$) is decomposed into two parts: the energies that are required for distorting the separate reactants (pyrrole nucleophile and Pd-allyl complex) from ground state to their transition state geometries [$\Delta E^{\ddagger}_{dist}$(pyrrole) and $\Delta E^{\ddagger}_{dist}$(Pd-allyl)], and the interaction energy between these deformed reactants ($\Delta E^{\ddagger}_{int}$). Thus, we have $\Delta E^{\ddagger}_{act} = \Delta E^{\ddagger}_{dist}$(pyrrole) $+ \Delta E^{\ddagger}_{dist}$(Pd-allyl) $+ \Delta E^{\ddagger}_{int}$.

The calculated distortion and interaction energies of the reactants in transition state geometries are listed in Table 3. For all six of the transition states that are listed in Figure 4, the distortion energies of pyrrole and Pd-allyl complex in the geometries of each transition states are very similar: 6.1−7.0 kcal/mol for $\Delta E^{\ddagger}_{dist}$(pyrrole) and 18.8−20.7 kcal/mol for $\Delta E^{\ddagger}_{dist}$(Pd-allyl). However, the interaction energies ($\Delta E^{\ddagger}_{int}$) of the two deformed reactants can be quite different for these transition states. For example, the $\Delta E^{\ddagger}_{int}$ of **TS-*endo*-*Re*-(-*sc*)** is −19.4 kcal/mol (entry 1), which is much more negative than those of the two transition states leading to (R) product [−15.1 kcal/mol for **TS-*endo*-*Re*-(+*sc*)**, entry 2, and −16.3 kcal/mol for **TS-*endo*-*Re*-(*ap*)**, entry 3]. The same trend is found for the three transition states for the formation of (S) product, in that **TS-*endo*-*Si*-(+*sc*)** enjoys the most significant interaction energy (−19.8 kcal/mol, entry 5) compared with the other two counterparts [−15.4 kcal/mol for **TS-*endo*-*Si*-(-*sc*)**, entry 4, and −15.8 kcal/mol for **TS-*endo*-*Si*-(*ap*)**, entry 6]. Apparently, the

much stronger interaction energy between the deformed pyrrole and Pd-allyl complex in **TS-*endo*-*Re*-(-*sc*)** and **TS-*endo*-*Si*-(+*sc*)** makes them the most stabilized transition states for the formation of (R) and (S) products, respectively.[31]

One common feature shared by **TS-*endo*-*Re*-(-*sc*)** and **TS-*endo*-*Si*-(+*sc*)** is that in these two lowest-energy transition states the nucleophile is approaching the Pd-allyl complex in such a trajectory that the pyrrole ring and the allyl moiety overlap with each other in the maximal way. Therefore, these structures might be further stabilized by secondary orbital interaction,[33] that is, the additional interaction between the orbitals located at the C4 and C5 position of the pyrrole ring and at the C2 and C3 position of the allyl moiety. In contrast, for the other four transition states whose energies are relatively higher, such favorable interaction is missing because the pyrrole ring just rotates away about the forming C−C bond (Figure 6). In other words, the secondary orbital interactions play an important role in the Pd-catalyzed asymmetric allylic dearomatization reactions by shaping the nucleophilic approaching trajectory to yield conformationally well-defined transition states.

On the basis of the above results, we have identified that **TS-*endo*-*Re*-(-*sc*)** and **TS-*endo*-*Si*-(+*sc*)** are the most stabilized transition states leading to (R) and (S) products, respectively. The calculated ΔG of **TS-*endo*-*Re*-(-*sc*)** is lower than that of **TS-*endo*-*Si*-(+*sc*)** by 1.9 kcal/mol. Since the interaction energies between the pyrrole nucleophile and the Pd-allyl complex are very similar for these two transition states (entries
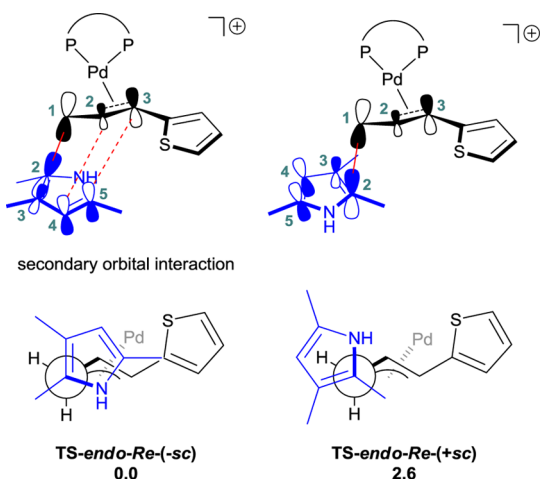
Figure 6. Schematic description of the secondary orbital interaction between the pyrrole ring and the allyl moiety (taking **TS-endo-Re-(-sc)** and **TS-endo-Re-(+sc)** as examples). The energies are in kcal/mol.

1 and 5, Table 3), there might be other reasons, probably steric effects, to account for the energetic difference. From the optimized structures of **TS-endo-Re-(-sc)** and **TS-endo-Si-(+sc)** shown in Figure 7, it can be found that, in both transition states, the steric interaction is not significant between the pyrrole ring and the phenyl groups of the chiral ligand which are stretching out. The shortest H···H distance between these two parts (H^3···H^6) is longer than 3 Å for both transition states [3.581 Å in **TS-endo-Re-(-sc)** and 3.175 Å in **TS-endo-Si-(+sc)**]. On the other hand, stronger steric repulsion between the allyl moiety and the incoming pyrrole ring in **TS-endo-Si-(+sc)** can be expected compared with **TS-endo-Re-(-sc)**, which is exemplified by some closer H···H distances in the former

transition state [$B(H^2 \cdots H^3) = 2.227$ Å, $B(H^1 \cdots H^4) = 2.386$ Å in **TS-endo-Si-(+sc)** vs $B(H^1 \cdots H^3) = 2.252$ Å, $B(H^2 \cdots H^5) = 2.409$ Å in **TS-endo-Re-(-sc)**]. Such an unfavorable interaction is reflected, to some extent, by the relatively higher distortion energies for both reactants in **TS-endo-Si-(+sc)** than **TS-endo-Re-(-sc)** (entry 5 vs entry 1, Table 3). The calculated results indicate that the (R) products should be formed preferentially, which is in line with the experimental observations.

■ CONCLUDING REMARKS

In this article, we present comprehensive DFT calculations on the Pd-catalyzed intermolecular asymmetric allylic dearomatization of multisubstituted pyrroles in the pursuit of a deep understanding of the remarkable regio- and enantioselectivity observed in this reaction. All the results presented here are well in agreement with the experimental observations. It was found that the regioselectivity is mainly governed by the HOMO distribution of the nucleophile. Among all the potential nucleophilic sites around the pyrrole ring, the reactions always occur at the position where the HOMO of the molecule is distributed most significantly. For the enantioselectivity, several factors are in operation. First, the chiral bisphosphine ligand arranges the Pd-allyl moiety in a certain configuration (endo), with only one face available for the nucleophilic attack. Second, although a collection of transition states with different conformations might exist due to the intermolecular nature of the reaction, the secondary orbital interaction between the pyrrole ring and the allyl moieties is found to be able to shape the approaching trajectory of the incoming nucleophile, and thus the most accessible transition state leading to (R) and (S) product, respectively, can be identified explicitly. Finally, the different steric repulsion between the pyrrole and allyl moieties observed in this two transition states discriminates the
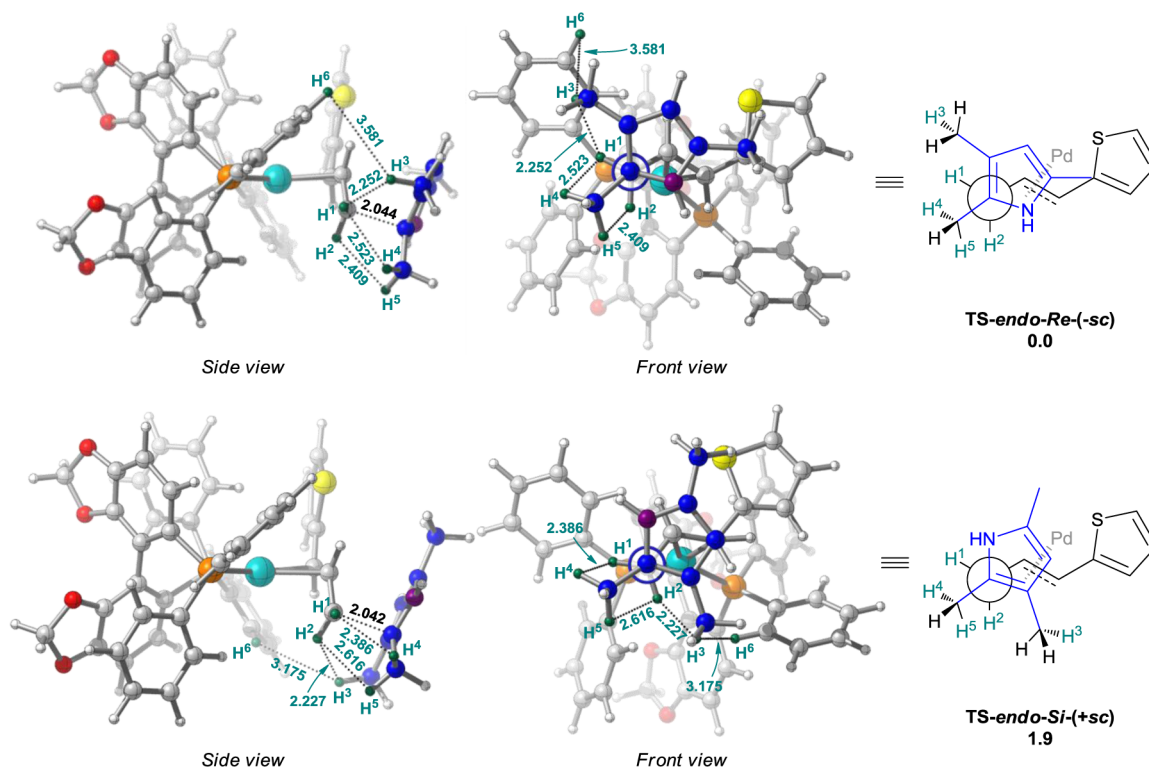
Figure 7. Optimized structures of **TS-endo-Re-(-sc)** and **TS-endo-Si-(+sc)**. The bond distances are in angstroms. The energies are in kcal/mol.

processes for the formation of the two enantiomers of the dearomatized products, with the (*R*)-2*H*-pyrroles being generated preferentially. In contrast to the common view on the origination of the enantioselectivity in Pd-catalyzed asymmetric allylic substitution reactions, the direct interaction between the chiral ligand and incoming nucleophile was not significant in the key transition states. The current study demonstrates the importance of the interaction between the allyl moiety and the π-system-containing nucleophiles. Since many nucleophiles which are widely used in Pd-catalyzed asymmetric allylic substitution reactions are π-systems, the secondary orbital interaction described here might also exist in many other cases and play a role in their chiral discrimination processes. The new insights gained from this work might help to refine the stereochemistry model of Pd-catalyzed asymmetric allylic substitution reactions and be beneficial for the future development of this field as well as the design of novel chiral ligands.

ASSOCIATED CONTENT

Ⓢ Supporting Information

Complete ref 18; full computational details including texts, figures, and Cartesian coordinates for all calculated stationary points. This material is available free of charge via the Internet at http://pubs.acs.org.

AUTHOR INFORMATION

Corresponding Authors
zhengchao@sioc.ac.cn
slyou@sioc.ac.cn

Notes
The authors declare no competing financial interest.

ACKNOWLEDGMENTS

REFERENCES

(1) Noyori, R. *Nat. Chem.* **2009**, *1*, 5.

(2) For reviews: (a) Balcells, D.; Maseras, F. *New J. Chem.* **2007**, *31*, 333. (b) Brown, J. M.; Deeth, R. J. *Angew. Chem., Int. Ed.* **2009**, *48*, 4476. (c) Fey, N. *Dalton Trans.* **2010**, *39*, 296. (d) Cheong, P. H.-Y.; Legault, C. Y.; Um, J. M.; Çelebi-Ölçüm, N.; Houk, K. N. *Chem. Rev.* **2011**, *111*, 5042.

(3) For reviews: (a) Trost, B. M.; Van Vranken, D. L. *Chem. Rev.* **1996**, *96*, 395. (b) Trost, B. M.; Crawley, M. L. *Chem. Rev.* **2003**, *103*, 2921. (c) Lu, Z.; Ma, S. *Angew. Chem., Int. Ed.* **2008**, *47*, 258. (d) Weaver, J. D.; Recio, A., III; Grenning, A. J.; Tunge, J. A. *Chem. Rev.* **2011**, *111*, 1846.

(4) For selected examples: (a) Sawamura, M.; Sudoh, M.; Ito, Y. *J. Am. Chem. Soc.* **1996**, *118*, 3309. (b) Sawamura, M.; Nakayama, Y.; Tang, W.-M.; Ito, Y. *J. Org. Chem.* **1996**, *61*, 9090. (c) Trost, B. M.; Radinov, R.; Grenzer, E. M. *J. Am. Chem. Soc.* **1997**, *119*, 7879. (d) You, S.-L.; Hou, X.-L.; Dai, L.-X.; Cao, B.-X.; Sun, J. *Chem. Commun.* **2000**, 1933. (e) Brunel, J. M.; Tenaglia, A.; Buono, G. *Tetrahedron: Asymmetry* **2000**, *11*, 3585. (f) Nemoto, T.; Matsumoto, T.; Masuda, T.; Hitomi, T.; Hatano, K.; Hamada, Y. *J. Am. Chem. Soc.* **2004**, *126*, 3690. (g) Nowicki, A.; Mortreux, A.; Agbossou-Niedercorn, F. *Tetrahedron: Asymmetry* **2005**, *16*, 1295.

(5) For selected examples: (a) Trost, B. M.; Schroeder, G. M. *J. Am. Chem. Soc.* **1999**, *121*, 6759. (b) You, S.-L.; Hou, X.-L.; Dai, L.-X.; Zhu, X.-Z. *Org. Lett.* **2001**, *3*, 149. (c) Trost, B. M.; Schroeder, G. M.;

Kristensen, J. *Angew. Chem., Int. Ed.* **2002**, *41*, 3492. (d) Trost, B. M.; Pissot-Soldermann, C.; Chen, I.; Schroeder, G. M. *J. Am. Chem. Soc.* **2004**, *126*, 4480. (e) Trost, B. M.; Schroeder, G. M. *Chem.—Eur. J.* **2005**, *11*, 174. (f) Zhang, K.; Peng, Q.; Hou, X.-L.; Wu, Y.-D. *Angew. Chem., Int. Ed.* **2008**, *47*, 1741. (g) Trost, B. M.; Malhotra, S.; Chan, W. H. *J. Am. Chem. Soc.* **2011**, *133*, 7328. (h) Trost, B. M.; Masters, J. T.; Burns, A. C. *Angew. Chem., Int. Ed.* **2013**, *52*, 2260.

(6) For selected examples: (a) Bélanger, É.; Cantin, K.; Messe, O.; Tremblay, M.; Paquin, J.-F. *J. Am. Chem. Soc.* **2007**, *129*, 1034. (b) Bélanger, É.; Pouliot, M.-F.; Courtemanche, M.-A.; Paquin, J.-F. *J. Org. Chem.* **2012**, *77*, 317.

(7) For selected examples: (a) Trost, B. M.; Ariza, X. *Angew. Chem., Int. Ed. Engl.* **1997**, *36*, 2635. (b) Trost, B. M.; Ariza, X. *J. Am. Chem. Soc.* **1999**, *121*, 10727. (c) Kawatsura, M.; Ikeda, D.; Ishii, T.; Komatsu, Y.; Uenishi, J. *Synlett* **2006**, 2435. (d) Di Giacomo, M.; Serra, M.; Brusasca, M.; Colombo, L. *J. Org. Chem.* **2011**, *76*, 5247.

(8) Asymmetric decarboxylative allylic alkylation reaction is another powerful strategy to construct an all-carbon stereogenic center in the incoming nucleophile moiety in asymmetric allylic alkylation reactions. For reviews: (a) You, S.-L.; Dai, L.-X. *Angew. Chem., Int. Ed.* **2006**, *45*, 5246. (b) Mohr, J. T.; Stoltz, B. M. *Chem.—Asian J.* **2007**, *2*, 1476. For selected examples: (c) Behenna, D. C.; Stoltz, B. M. *J. Am. Chem. Soc.* **2004**, *126*, 15044. (d) Trost, B. M.; Xu, J. *J. Am. Chem. Soc.* **2005**, *127*, 2846. (e) Mohr, J. T.; Behenna, D. C.; Harned, A. M.; Stoltz, B. M. *Angew. Chem., Int. Ed.* **2005**, *44*, 6924. (f) Nakamura, M.; Hajra, A.; Endo, K.; Nakamura, E. *Angew. Chem., Int. Ed.* **2005**, *44*, 7248. (g) Kuwano, R.; Ishida, N.; Murakami, M. *Chem. Commun.* **2005**, 3951. (h) Trost, B. M.; Bream, R. N.; Xu, J. *Angew. Chem., Int. Ed.* **2006**, *45*, 3109. (i) Trost, B. M.; Xu, J.; Reichle, M. *J. Am. Chem. Soc.* **2007**, *129*, 282. (j) Enquist, J. A.; Stoltz, B. M. *Nature* **2008**, *453*, 1228. (k) Bélanger, É.; Houzé, C.; Guimond, N.; Cantin, K.; Paquin, J.-F. *Chem. Commun.* **2008**, 3251. (l) Trost, B. M.; Xu, J.; Schmidt, T. *J. Am. Chem. Soc.* **2009**, *131*, 18343. (m) Behenna, D. C.; Liu, Y.; Yurino, T.; Kim, J.; White, D. E.; Virgil, S. C.; Stoltz, B. M. *Nat. Chem.* **2012**, *4*, 130. (n) Reeves, C. M.; Eidamshaus, C.; Kim, J.; Stoltz, B. M. *Angew. Chem., Int. Ed.* **2013**, *52*, 6718. (o) Kaiser, T. M.; Yang, J. *Eur. J. Org. Chem.* **2013**, 3983.

(9) Chiral counteranion-directed catalysis has also been employed in Pd-catalyzed asymmetric allylic substitution reactions with prochiral nucleophiles to construct all-carbon quaternary stereogenic centers: (a) Mukherjee, S.; List, B. *J. Am. Chem. Soc.* **2007**, *129*, 11336. (b) Jiang, G.; List, B. *Angew. Chem., Int. Ed.* **2011**, *50*, 9471. (c) Ohmatsu, K.; Ito, M.; Kunieda, T.; Ooi, T. *Nat. Chem.* **2012**, *4*, 473. (d) Ohmatsu, K.; Ito, M.; Kunieda, T.; Ooi, T. *J. Am. Chem. Soc.* **2013**, *135*, 590.

(10) For the working model of predicting the stereochemistry of the Pd-catalyzed asymmetric allylic substitution reaction involving Trost ligands: Trost, B. M.; Machacek, M. R.; Aponick, A. *Acc. Chem. Res.* **2006**, *39*, 747 and references cited therein.

(11) Butts, C. P.; Filali, E.; Lloyd-Jones, G. C.; Norrby, P.-O.; Sale, D. A.; Schramm, Y. *J. Am. Chem. Soc.* **2009**, *131*, 9945.

(12) Kleimark, J.; Norrby, P.-O. *Top. Organomet. Chem.* **2012**, *38*, 65 and references cited therein.

(13) For reviews on dearomatization reactions: (a) Pape, A. R.; Kaliappan, K. P.; Kündig, E. P. *Chem. Rev.* **2000**, *100*, 2917. (b) López Ortiz, F.; Iglesias, M. J.; Fernández, I.; Andújar Sánchez, C. M.; Gómez, G. R. *Chem. Rev.* **2007**, *107*, 1580. (c) Roche, S. P.; Porco, J. A., Jr. *Angew. Chem., Int. Ed.* **2011**, *50*, 4068. (d) Zhuo, C.-X.; Zhang, W.; You, S.-L. *Angew. Chem., Int. Ed.* **2012**, *51*, 12662. (e) Ding, Q.; Ye, Y.; Fan, R. *Synthesis* **2013**, *45*, 1. For a review on transition-metal-catalyzed asymmetric allylic dearomatization reactions: (f) Zhuo, C.-X.; Zheng, C.; You, S.-L. *Acc. Chem. Res.* **2014**, *47*, 2558.

(14) (a) Kimura, M.; Futamata, M.; Mukai, R.; Tamaru, Y. *J. Am. Chem. Soc.* **2005**, *127*, 4592. (b) Trost, B. M.; Quancard, J. *J. Am. Chem. Soc.* **2006**, *128*, 6314. (c) Zhang, X.; Yang, Z.-P.; Liu, C.; You, S.-L. *Chem. Sci.* **2013**, *4*, 3239. (d) Zhuo, C.-X.; You, S.-L. *Angew. Chem., Int. Ed.* **2013**, *52*, 10056. (e) Liu, Y.; Du, H. *Org. Lett.* **2013**, *15*, 740. (f) Zhang, X.; Han, L.; You, S.-L. *Chem. Sci.* **2014**, *5*, 1059.

(15) Zhuo, C.-X.; Zhou, Y.; You, S.-L. *J. Am. Chem. Soc.* **2014**, *136*, 6590.

(16) For intramolecular asymmetric allylic dearomatization reactions of pyrroles: (a) Zhuo, C.-X.; Liu, W.-B.; Wu, Q.-F.; You, S.-L. *Chem. Sci.* **2012**, *3*, 205. (b) Zhuo, C.-X.; Wu, Q.-F.; Zhao, Q.; Xu, Q.-L.; You, S.-L. *J. Am. Chem. Soc.* **2013**, *135*, 8169.

(17) (a) Kuwano, R.; Ito, Y. *J. Am. Chem. Soc.* **1999**, *121*, 3236. (b) Kuwano, R.; Nishio, R.; Ito, Y. *Org. Lett.* **1999**, *1*, 837. (c) Kuwano, R.; Uchida, K.-i.; Ito, Y. *Org. Lett.* **2003**, *5*, 2177. (d) Ogasawara, M.; Ngo, H. L.; Sakamoto, T.; Takahashi, T.; Lin, W. *Org. Lett.* **2005**, *7*, 2881.

(18) Frisch, M. J.; et al. *Gaussian09*, Revision D.01; Gaussian, Inc.: Wallingford, CT, 2013.

(19) (a) Zhao, Y.; Truhlar, D. G. *Theor. Chem. Acc.* **2008**, *120*, 215. (b) Zhao, Y.; Truhlar, D. G. *Acc. Chem. Res.* **2008**, *41*, 157.

(20) Marenich, A. V.; Cramer, C. J.; Truhlar, D. G. *J. Phys. Chem. B* **2009**, *113*, 6378.

(21) (a) Becke, A. D. *J. Chem. Phys.* **1993**, *98*, 5648. (b) Lee, C.; Yang, W.; Parr, R. G. *Phys. Rev. B* **1988**, *37*, 785.

(22) Grimme, S.; Ehrlich, S.; Goerigk, L. *J. Comput. Chem.* **2011**, *32*, 1456.

(23) (a) Hujo, W.; Grimme, S. *Phys. Chem. Chem. Phys.* **2011**, *13*, 13942. (b) Goerigk, L.; Kruse, H.; Grimme, S. *ChemPhysChem* **2011**, *12*, 3421. (c) Kruse, H.; Goerigk, L.; Grimme, S. *J. Org. Chem.* **2012**, *77*, 10824. (d) Ehrlich, S.; Moellmann, J.; Grimme, S. *Acc. Chem. Res.* **2013**, *46*, 916. (e) Jindal, G.; Sunoj, R. B. *Angew. Chem., Int. Ed.* **2014**, *53*, 4432.

(24) Lu, T.; Chen, F. *J. Comput. Chem.* **2012**, *33*, 580.

(25) Legault, C. Y. *CYLView*, 1.0b; Université de Sherbrooke, Montreal, Québec, Canada, 2009; http://www.cylview.org.

(26) (a) Noyori, R. *Science* **1990**, *248*, 1194. (b) Ozawa, F.; Kubo, A.; Matsumoto, Y.; Hayashi, T.; Nishioka, E.; Yanagi, K.; Moriguchi, K. *Organometallics* **1993**, *12*, 4188.

(27) Boele, M. D. K.; Kamer, P. C. J.; Lutz, M.; Spek, A. L.; de Vries, J. G.; van Leeuwen, P. W. N. M.; van Strijdonck, G. P. F. *Chem.—Eur. J.* **2004**, *10*, 6232.

(28) (a) Lloyd-Jones, G. C.; Stephen, S. C. *Chem.—Eur. J.* **1998**, *4*, 2539. (b) Lloyd-Jones, G. C.; Stephen, S. C.; Murray, M.; Butts, C. P.; Vyskočil, Š.; Kočovský, P. *Chem.—Eur. J.* **2000**, *6*, 4348.

(29) The calculated ee value of the product **3cb** is also 92% if only the two most stabilized transition states **TS-*endo*-*Re*-(-*sc*)** and **TS-*endo*-*Si*-(+*sc*)** are considered.

(30) For reviews on activation strain model: (a) van Zeist, W.-J.; Bickelhaupt, F. M. *Org. Biomol. Chem.* **2010**, *8*, 3118. (b) Fernández, I.; Bickelhaupt, F. M. *Chem. Soc. Rev.* **2014**, *43*, 4953. For selected examples on application of activation strain model in transition-metal-catalyzed reactions: (c) de Jong, G. T.; Bickelhaupt, F. M. *ChemPhysChem* **2007**, *8*, 1170. (d) Legault, C. Y.; Garcia, Y.; Merlic, C. A.; Houk, K. N. *J. Am. Chem. Soc.* **2007**, *129*, 12664. (e) Gorelsky, S. I.; Lapointe, D.; Fagnou, K. *J. Am. Chem. Soc.* **2008**, *130*, 10848. (f) Liu, P.; McCarren, P.; Cheong, P. H.-Y.; Jamison, T. F.; Houk, K. N. *J. Am. Chem. Soc.* **2010**, *132*, 2050. (g) Green, A. G.; Liu, P.; Merlic, C. A.; Houk, K. N. *J. Am. Chem. Soc.* **2014**, *136*, 4575.

(31) Activation strain diagrams showing the potential energy $\Delta E_{act}(\zeta)$, the distortion energies of both reactants $\Delta E_{dist}(\zeta)$(Pd-allyl) and $\Delta E_{dist}(\zeta)$(pyrrole), and the interaction energy $\Delta E_{int}(\zeta)$ as a function of the reaction coordinate (ζ) are given in the Supporting Information. The interaction energies $\Delta E_{int}(\zeta)$ of **TS-*endo*-*Re*-(-*sc*)** and **TS-*endo*-*Si*-(+*sc*)** are more negative than those of the other four transition states at any given point along the reaction coordinate.

(32) Hartwig, J. F. *Organotransition metal chemistry: from bonding to catalysis*; University Science Books: Sausalito, CA, 2010; p 265.

(33) For selected reviews on secondary orbital interactions: (a) Ginsburg, D. *Tetrahedron* **1983**, *39*, 2095. (b) García, J. I.; Mayoral, J. A.; Salvatella, L. *Acc. Chem. Res.* **2000**, *33*, 658. For an early example which suggests the secondary orbital interaction is involved in determining the regioselectivity of Mo-catalyzed allylic substitution reactions: (c) Malkov, A. V.; Davis, S. L.; Baxendale, I. R.; Mitchell, W. L.; Kočovský, P. *J. Org. Chem.* **1999**, *64*, 2751.